Nanoscale

Accepted Manuscript

This article can be cited before page numbers have been issued, to do this please use: E. B. Kang, J. Lee, Z. A. I. Mazrad, I. In, J. H. Jeong and S. Y. Park, *Nanoscale*, 2017, DOI: 10.1039/C7NR07900A.

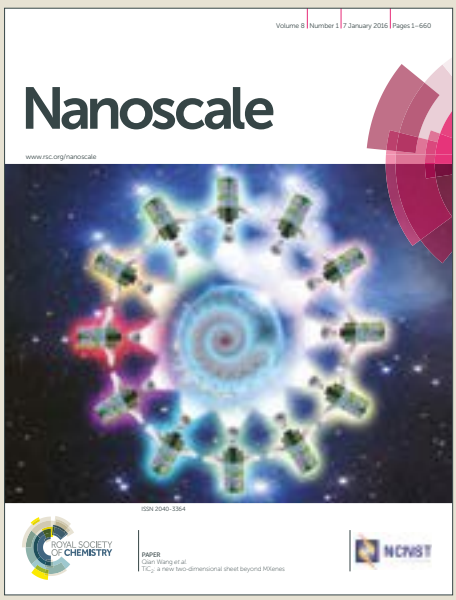

ROYAL SOCIETY OF CHEMISTRY

rsc.li/nanoscale

View Article Online
DOI: 10.1039/C7NR07900A

Nanoscale

ARTICLE

pH-Responsible Fluorescent Carbon Nanoparticles for Tumor Selective Theranostics via pH-turn on/off Fluorescence and Photothermal Effect *In Vivo* and *In Vitro*

Received 00th January 20xx,
Accepted 00th January 20xx

DOI: 10.1039/x0xx00000x

www.rsc.org/

Eun Bi Kang[a]†, Jung Eun Lee[b]†, Zihnil Adha Islamy Mazrad[c], Insik In[c, d], Ji Hoon Jeong[b]*, Sung Young Park[a, c]*

We developed nanoparticles comprising a photothermal dye (IR825)-loaded carbonized zwitterionic polymer [FNP-I], as "switch-on" pH-responsive fluorescence probes to sense intracellular cancer cell and for near infrared (NIR) controllable photothermal therapy (PTT) in vivo and in vitro. The fluorescent "off" of FNP-I is activated after reaching the cancer cell environment, where the zwitterionic compartment of FNP will lose its hydrophobicity to induce PTT-mediated heat release of IR825 under NIR irradiation in the tumor. Approximately 100% of the IR825 was released from the FNP core to generate high thermal conversion for the complete killing of cancer cells. Furthermore, after intravenous treatment of FNP-I into MDAMB-231-cell bearing mice, pH responsive photothermal therapy was observed, achieving marked ablation of tumor cells with release of IR825 under tumor environment conditions. In addition, fluorescent signals were clearly found in the tumor site after 3 h, decreasing at the 6 h time point. The in vitro and in vivo detection system demonstrated good cellular uptake and biocompatibility as potential imaging-guided photothermal therapy nanotool for cancer treatment. Interestingly, the synergism of the biosensor and PTT in single FNP-I platform led to more effective cancer cell killing than either monotherapy, providing a new approach for cancer treatment.

Introduction

The principal goal of the battle with cancer is to developing effective therapeutic strategies with high specificity and few side effects. In particular, the therapy should treat metastases, further prevent their recurrence, achieve better tumor targeting, and low be non-toxic to normal cells.[1,2] Currently, nanomaterials have become a research focus, particularly in cases where the gold-standard cancer treatments, surgery, chemotherapy, and radiotherapy, fail to eradicate the cancer cells.[3, 4] In recent years, in addition to our increasing knowledge concerning cancers, photothermal heating has shown promise as a next generation method to overcome the limitation of traditional chemotherapeutics.[4] Thus, photothermal therapy (PTT) has been developed as a new strategy that employs the heat generated from the absorbed optical energy (600—900 nm) by light-absorbing agents that are accumulated in the tumor to ablate tumor cells.[5-7]

Improvements to therapeutic delivery requires nanoparticle that respond to both exogenous (temperature, light, magnetic/electric field, and ultrasound) and endogenous (changes in pH, redox potential, and concentrations of enzymes) stimuli to achieve effective delivery into the specific targeted cancer.[8-10] In the tumor environment, the tumor cells have a pH range around 6.5–6.9, and the pH of endosomes is around 5.0 for endosomes, which differ from normal cells.[10] Therefore, pH responsive nanoparticles can be used to detect the cancer cells by taking into account the microenvironment. As a result, zwitterionic molecules, which possess cationic and anionic groups to control the surface charge by pH in buffer solutions, have been developed.[11, 12] At acidic pH, they have a positive charge and in basic conditions they have a negative charge; at pH 7.4 they have no charge, which makes them more hydrophobic. Once the zwitterionic material enters a tumor cell, they respond to the pH environment in the cell by changing their conformation to release the therapeutic agent.[12]

[a] Department of Chemical & Biological Engineering, Korea National University of Transportation, Chungju 380-702, Republic of Korea
[b] School of Pharmacy, Sungkyunkwan University, 300 Cheoncheon-dong, Jangan-gu, Suwon, Gyeonggi-do 440-746, Republic of Korea.
[c] Department of IT Convergence, Korea National University of Transportation Chungju 380-702, Republic of Korea.
[d] Department of Polymer Science and Engineering, Korea National University of Transportation, Chungju 380-702, Republic of Korea.

*Corresponding authors: parkchem@ut.ac.kr; E-mail:jhjeong@skku.edu
Electronic Supplementary Information (ESI) available: See DOI: 10.1039/x0xx00000x

View Article Online
DOI: 10.1039/C7NR07900A

For cancer cell detection, fluorescence assays based on on/off systems have been developed.[13-14] Fluorescence assays are often highly favored over other techniques because of their high selectivity, low cost, and simplicity, and they can be applied without the use of sophisticated equipment. Hence, fluorescent carbon nanoparticles (FNPs), as fluorescent probes for intracellular cancer sensing, have favorable properties, including low cost, high quantum yield, water solubility, low toxicity, good photostability, and excellent biocompatibility.[15-17] Furthermore, FNPs contain many π-π bonds that permit drug loading through strong π-π-stacking or via hydrophobic interaction for aromatic molecules; therefore, FNPs are useful as transporters for therapeutic agents.[15]

Previously, it was revealed that near infrared (NIR)-absorbing dyes, such as indocyanine green (ICG), IR780, and IR825 can produce excellent photothermal conversion efficiencies for PTT.[18-22] However, the use of single dyes without other conjugation materials is a challenge because of their poor aqueous stability or solubility. In this regard, loading these dyes into nanocarriers could not only improve their aqueous solubility and prolong their blood circulation time, but also quench the FNPs through the Förster resonance energy transfer (FRET) for fluorescence on/off assays. Combining organic dyes with FNPs results in energy transfer, with changes in the fluorescence excitation and/or emission spectra, which induces fluorescence turn off.[14]

Previous studies conjugated the targeting agent to the matrix to achieve good uptake by cancer cells. Nano-sized carbonized polymers tend to remain in blood circulation for long time when administered intravenously. Their small size means that the agents passively penetrate into the tumor tissue through the enhanced permeability and retention (EPR) effect.[23] Most nano-sized agents accumulate within tumors because of the EPR effect and then release their therapeutic payloads.[23] Based on this effect, the carbonized system can reduce the complexity of the matrix to enhance internalization of an agent within the tumor cell.

In this study, we synthesized pH imaging and pH-responsive PTT nanoparticles (FNP-I) that are effective for tumor therapy, comprising carbonized cross-linked poly(ethylene glycol-g-poly(sulfobetaine methacrylate) loaded with IR825 (loaded using π-stacking or hydrophobic interaction in neutral condition).[24] When not at the tumor site, FNP-I fluorescence is quenched. After reaching the tumor site, the NIR-absorbing IR825 is released from the nanoparticle, allowing recovery of FNP-I fluorescent behavior and the induction of photothermal cytotoxicity after external NIR light exposure simultaneously, under different pH conditions. The results revealed that FNP-I could not only release the agent at the appropriate tumor site, but also possessed high efficiency of heat conversion under NIR irradiation with good cellular uptake. Thus, we developed a superior system for simultaneous diagnosis and phototherapy against malignant tumors by exploiting a fluorescence on/off assay in response to the pH of the tumor cell environment.

Experimental

Materials

Polyethylene glycol (PEG), 2-dimethylaminoethyl methacrylate (DMA), 2-2′-azobis(isobutyronitrile) (AIBN), 2-mercaptoethanol (CTA), bromoethane, ethanol, 1,3-propanesultone, methanol, dimethyl sulfoxide (DMSO), tert-Butyl peroxybenzoate, toluene, H_2SO_4, and [3-(4,5-dimethylthiazol-2-yl)-2,5-diphenyltetrazolium bromide] (MTT) were purchased from Sigma-Aldrich, Seoul, Korea. Penicillin–streptomycin, fetal bovine serum (FBS), 0.25% (w/v) Trypsin, 0.03% (w/v) EDTA (ethylenediaminetetraacetic acid) solution, and Roswell Park Memorial Institute (RPMI)-1640 medium were purchased from Gibco BRL (Carlsbad, CA, USA). Female nude mice (BALB/c nu/nu) were purchased from Daehan Biolink Co. Ltd. (Korea) and used at 6 weeks of age. All animal procedures were performed in accordance with the Guidelines for Care and Use of Laboratory Animals of Sungkyunkwan University in Republic of Korea and approved by the Animal Ethics Committee of the Institutional Animal Care and Use Committee (IACUC). The heptamethine dye IR825 was synthesized using a previously reported protocol.[24]

Carbonization of polyethylene glycol grafted poly(sulfobetaine methacrylate) [FNP]

Polyethylene glycol-g-poly(sulfobetaine methacrylate) (PSM) was synthesized according to a previously reported method.[12] To obtain the FNP, PSM (1 g) was dissolved in DI Millipore water (5 mL) at 25 °C. To this solution, 10 mL of 36 N H_2SO_4 was added and stirred for 1 minute.[15] The final reaction was added to 185 mL double-distilled water (DDW) and dialyzed using a membrane (molecular

View Article Online
DOI: 10.1039/C7NR07900A

weight cut off (MWCO): 1000) in water. Finally, the product was freeze-dried and collected.

IR825 Loading (FNP-I)

FNP containing IR825 were prepared as follows: 100 mg of FNP was dissolved in 20 mL of pH 7.4 phosphate buffered saline (PBS) solution. To load IR825, 1 mg of IR825 dissolved in DMSO was poured into the FNP solution and stirred for 1 day at room temperature (19–21 °C). The solution was then dialyzed against PBS for 24 h. The solution was then filtered through a 0.45-µm micro filter to eliminate the non-complexed IR825 and aggregated particles. The loading efficiency = [IR825(total) – IR825(noncomplex)] × 100/[IR825(total)], and was found to be 89.9%.

***In vitro* IR825 release under different pH environments**

IR825 release was evaluated using UV-vis spectroscopy. Briefly, the samples were dialyzed against phosphate buffer solution at 37 °C. The MWCO (1000) of the semipermeable membrane allowed the IR825 molecules to be transported between the inside and the outside of the dialysis chamber, while the FNP were retained in the dialysis bag. Next, 3 mL of FNP-I solution was placed in three individual dialysis chambers and each chamber was treated with different pH. Tween 80 was added outside the dialysis chamber as a surfactant. The sample solutions were dialyzed in a shake incubator at 37 °C during the whole experimental period. After 24 h, 3 mL of the IR825 released solution was collected from outside the membrane to measure the amount of IR825 released, and 3 mL fresh buffer solution was replaced to keep the volume constant. The samples were then observed using UV-Vis spectroscopy. In the experiment, the experimental parameters were constant for the same group of samples.

Reversible behavior of FNP-I nanoparticles

The FNP-I in 1 mg/mL concentration was firstly dilute at pH 7.4 solution and the fluorescent properties of the sample were then observed using PL spectroscopy. The used sample was next freeze-dried for 1 day. The dried sample from freeze drying was collected to dilution in pH 6.8 solution. Next, the solution was rechecked via PL spectroscopy. The subsequent experiment were followed the above method for 7 cycles.

MTT assay

Cytotoxicity was measured using the MTT assay. KB cells, MDAMB-231 cells, and MDCK cells (all 200 µL) at a density of 1×10^5 cells/mL were placed in each well of a 96-well plate. The cells were incubated for 24 h at 37 °C in a 5% humidified CO_2 atmosphere. To determine the cell viability, stock solutions of FNP and FNP-I were dissolved in RPMI medium at a concentration of 1 mg/mL and diluted up to 0.001 mg/mL. The media was removed, and the cells were treated with different concentrations of FNP and FNP-I. The cells were then incubated for another 24 h. The media containing FNP and FNP-I were then replaced with 180 µL fresh medium and 20 µL of a stock solution containing 15 mg of MTT in 3 mL of PBS and incubated for another 4 h. Finally, the medium was removed and 200 µL of MTT solubilizing agent was added to the cells, and the reaction mixture was shaken for 15 min. Absorbance was measured at a 570 nm using a microplate reader. The relative cell viability was measured by comparing the results for the samples with that of the control well containing cells only.

Confocal imaging

The cellular uptake of the composite materials was analyzed using confocal imaging. MDAMB-231 cells were plated over a cover slide on an eight-well plate at a density of 2 × 105 cells/mL per well and incubated for 24 h at 37 °C in a 5% humidified CO2 atmosphere. The cells were then treated with the FNP-I and Lysotracker at 0.01 mg/mL for 30 min in fresh culture medium. The medium was washed off with PBS several times to remove the unbound FNP-I. Finally, the cells were examined at 20× magnification using an LSM510 confocal laser scanning microscope (Carl Zeiss, Germany).

***In vivo* bioimaging**

Tumor-bearing mice were generated by intravenous injection of MDAMB-231 cells (1×10^7 cells) into one of the flank regions each mouse. Tumor-bearing mice were injected intravenously with 50 µL of FNP-I and imaged using an *in vivo* fluorescence imaging system (VISQUE™ In vivo Elite, Vieworks) at different times post injection. To investigate the biodistribution of the particles, tumor-bearing mice were sacrificed at 3 h post injection and the tumor and major organs (heart, liver, spleen, lungs, and kidneys) were harvested. Each organ was rinsed with PBS, sectioned, mounted on slides, and

View Article Online
DOI: 10.1039/C7NR07900A

examined under a confocal laser-scanning microscope (Zeiss LSM 710).

***In vivo* photothermal therapy and histology**

To investigate the antitumor effect of FNP-I, MDAMB-231 cells were freshly harvested (1× 10^7 per mouse) and injected into mice. When the tumor size was reached approximately 100 mm^3, mice were treated with FNP-I at concentration 10 mg/kg (body weight). Tumor volumes were continuously monitored for 12 days after tumor cell inoculation. The tumor tissues were irradiated with a 808 nm laser (2 W/cm^2) for 5 min at 2 h post injection. Tumor volumes were calculated using longitudinal (L) and transverse (W) tumor diameters, according to the formula V = (L x W^2)/2. *In vivo* images were taken using an *in vivo* fluorescence imaging system (VISQUE™ InVivo Elite, Vieworks) post injection.

At 24 h after FNP-I injection, tumor tissues were recovered from euthanized animals for histochemical evaluation. Tissue sections (4 μm) were cut from 10% neutral buffered formalin-fixed and paraffin-embedded tissue blocks and stained with hematoxylin and eosin (H&E) to determine the *in vivo* cytotoxic effect.

Characterization

^{1}H-NMR spectra were recorded using a Bruker Advance 400 MHz spectrometer with deuterated dimethyl sulfoxide (d_6-DMSO) as the solvent. The ultraviolet-visual (UV–vis) spectra were recorded using an Optizen 2120 UV spectrophotometer (Mecasys Co). Particle size was measured using dynamic light scattering (DLS) (Zetasizer Nano, Malvern-Germany). The X-ray photoelectron spectroscopy (XPS) results were obtained using an Omicrometer ESCALAB (Omicrometer, Taunusstein, Germany), and the Photoluminescence (PL) spectra were obtained using an FluoroMate fluorometer from Scinco. A multimode microplate reader, Filter MaxF3 (Varioskan Flash, Thermo Electron Corp., Waltham, MA, USA), was used for the MTT assay. Fluorescence lifetimes were measured using a NanoLED laser light source (Horiba Jobin Yvon NanoLog spectrophotometer) at 375 nm for excitation, and the data were fitted using a multi-exponential decay model. Transmission electron microscopy (TEM, JEM-2100F, JEOL) was carried out using an electron gun with a potential in the range of 80–200 kV. Confocal laser scanning microscopy (CLSM) images of the samples were recorded using an LSM510 confocal microscope (Carl Zeiss, Oberkochen 73447, Germany).

Result and discussion

In this study, we formed zwitterionic groups via betanization of the amine terminal groups of PEG-g-PDMA with 1,3-propanosultone through the ring-opening reaction, followed by further carbonization, to form pH responsive fluorescent nanoparticles (FNP) (Scheme 1). The pH sensitive zwitterionic FNP can control the release of a therapeutic payload as a photothermal cancer therapy and can detect the target cancer through fluorescence on/off assay by controlling the release of IR825 as quencher/photothermal dye.

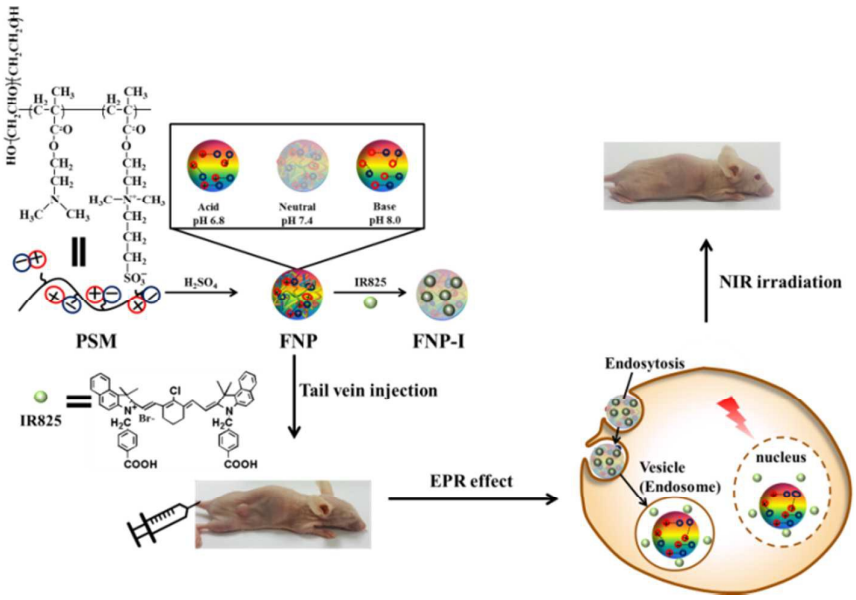

View Article Online
DOI: 10.1039/C7NR07900A

Scheme 1. Schematic diagrams of IR825 loaded pH reversible zwitterionic fluorescent nanoparticles for tumor detection and guided photothermal cancer therapy *in vitro* (a) and *in vivo* (b).

The chemical structure of the zwitterionic groups and IR825 loading were characterized by ^{1}H-NMR (Figure 1). The sultone peaks were detected at 2.0~3.3 ppm in the PEG-g-PDMA polymer backbone, at 3.5 ppm for PEG, and at 1.0 ppm for PDMA.[25] In addition, the intense peak at 7.0–8.5 ppm represented the aromatic groups of the NIR responsive IR825 loaded into the core of the FNP.[26] This peak disappeared after pH shock at 6.0 to mimic the pH of cancer cells. The disappearance of the IR825 peak was caused by changes to zwitterionic groups at pH 6.0; they become more hydrophilic, which opens up their structure, allowing the release of IR825 from the core. We also confirmed the successful loading of IR825 using UV-Vis spectroscopy analysis. In the UV-Vis spectrum, the absorbance peak of FNP showed broad absorption properties at 300-400 nm, indicating the π-π* bonds in carbonized material.[27] The strong peak at 700–825 nm at pH 7.4 of the FNP-I confirmed that IR825 could be loaded by hydrophobic intercalation between the hydrophobic zwitterionic moieties at pH 7.4 with the high loading efficiency around 89.9%.[26, 28] Similar to the NMR data, the IR825 peak in the UV-vis spectrum disappeared at pH 6. This phenomenon can be rationalized by the deprotonation of the zwitterionic groups, making them suitable for use as pH responsive nanocarriers.

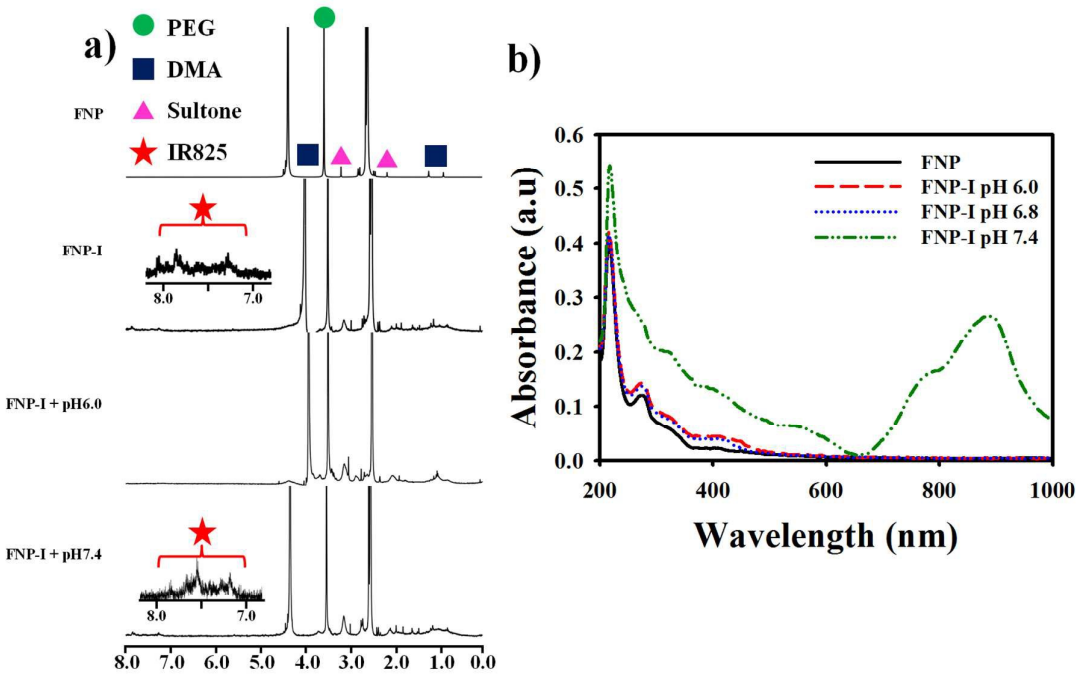

Figure 1. (**a**)^{1} H NMR spectra in DMSO of FNP and FNP-I after pH treatment (**b**) The UV–vis absorption spectra of FNP, FNP-I and FNP-I with different pH conditions (Concentration: 0.1 mg/ml in DDW). NMR, nuclear magnetic resonance; FNP, fluorescent nanoparticle; FNP-I, FNP loaded with IR825; DMSO, dimethyl sulfoxide; UV-via, ultraviolet-visual; PEG, polyethylene glycol; DMA, 2-dimethylaminoethyl methacrylate.

In addition, Figure S1 shows the chemical elemental composition of the FNP, as confirmed by XPS analysis. In the wide-scan XPS spectrum, the peaks of carbon (C 1s), nitrogen (N 1s), and oxygen (O 1s) elements appeared at 289, 401, and 532 eV, respectively. The narrow-scan C1s spectra of the FNPs showed different carbon groups, including C=C, C-C, C-O, C-O-C, C=O, and O-C=O at around 283.8, 284.2, 286, 287, 288.2, and 289.5 eV, respectively. The presence of an S2p peak at 168 eV represents the sultone groups in

View Article Online
DOI: 10.1039/C7NR07900A

the FNP core. The high-resolution and narrow element spectra provided evidence of the correct chemical structure of the FNP.

At pH 7.4, the size of the FNP was determined as 30 nm via DLS measurement. At pH 6.0 and 6.8, the size of the FNP decreased, indicating the breakdown of the aggregation of zwitterion groups. For the FNP-I, with the zwitterionic sulfobetaine group of FNP and the IR825 dye applied within the hydrophobic inner core, the particle size was determined as 130 nm at pH 7.4. Under acid conditions, the size of the FNP-I was similar to that of the FNP in acid conditions because of protonation of the sulfobetaine groups, which results in the cationic form of FNP and increased hydrophilicity through breakdown of the aggregated structure. Furthermore, as shown in Figure 2b, the TEM images of FNP and FNP-I showed a dot-shaped morphology with similar sizes to those determined by DLS measurement at different pH conditions. Carbonization caused our FNP to form a lattice structure, as shown by high-resolution TEM (HR-TEM) images on Figure 2b. They showed a lattice spacing of 0.33–0.34 nm, confirming a graphene lattice structure.[27] For advanced analysis, we conducted powder X-ray diffraction (PXRD) to support the lattice assignments in Figure S2. Figure S2 show two intense peaks at around 2θ = 12.9° and 24.7°, which corresponds to a d spacing of 0.32-0.362 nm and indicates the graphitic stacking with an interlayer.[29]

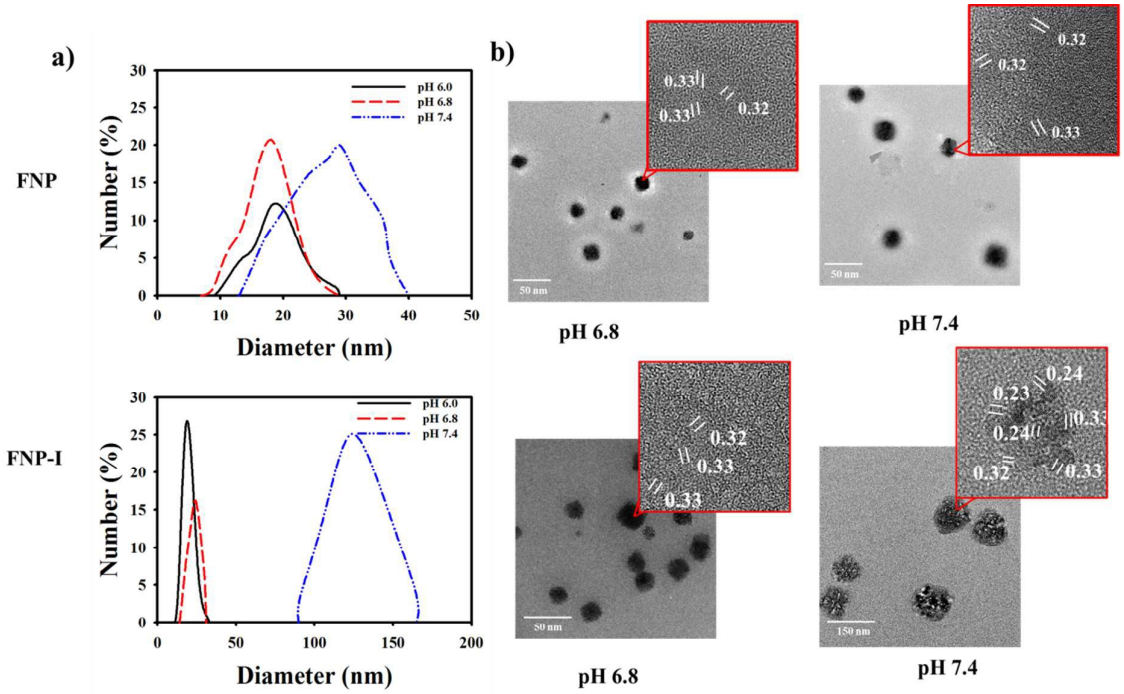

Figure 2. (**a**) Dynamic light scattering (DLS) measurements (**b**) The transmission electron microscopy (TEM) images of FNP and FNP-I under different PBS solution, pH 6.8 and 7.4). FNP, fluorescent nanoparticle; FNP-I, FNP loaded with IR825; PBS, phosphate buffered saline.

As shown in Scheme 1, we hypothesized that the fluorescence characteristics of the prepared FNP would depend on the zwitterionic polysulfobetaine group; i.e., protonation in the acidic environment and deprotonation under base conditions, to produce FNP with a highly hydrophilic nature. We measured the zeta potential to confirm this tendency (Figure S3). In an acidic environment of pH 5.0, the zeta potential was +7.62 mV and at pH 6.0 it was +8.14 mV, indicating the cationic nature of the zwitterionic FNP. However, at neutral pH values, the zeta potential was decreased to reflect the neutral or non-ionized form. To track the nanocarriers within a bio-system, we employed the different pH condition between cancer and normal cell to explore the fluorescent profile based on the pH effect.

View Article Online
DOI: 10.1039/C7NR07900A

The fluorescence quenching effect of IR825 was studied using a Stern-Volmer plot with different amounts of quencher loaded on the FNP.[27, 30, 31] Figure S4 shows that the fluorescence decreased as the amount of quencher increased. The graph plotting of the ratio of the initial fluorescence (F_0) to the final fluorescence (F) (F_0/F) revealed that the quenching intensity correlated with the concentration of the quencher, which could be caused either by FRET or static quenching through donor and acceptor behavior. Figure S5 shows that there was no detectable fluorescence of FNP at pH 7.4 because of self-quenching, which resulted from the formation of neutral sultone groups, compared with the fluorescence observed at pH 6.0 and 6.8. Furthermore, the applying IR825 into the FNP core produced similar fluorescent behavior to that of the naked FNP at different pH with the fluorescent ratio between FNP and FNP-I at acidic pH was found to be 1:0.8. Although the fluorescent profiles in response to pH were almost the same, loading IR825 into the core increased the quenching effect at pH 7.4. This was probably caused by the capture of IR825 by the hydrophobic sultone moieties at pH 7.4, resulting in energy transfer through FRET. In the Figure S5 we can also clearly see the peak of IR825 under pH 6.0 and 6.8 at wavelength ~550 nm while cannot be find at pH 7.4, confirming the strong encapsulation of IR825 inside the FNP core and relieve at acidic condition. In particular, at below pH 7.4 the sultone groups on FNP surfaces are protonated and ionized on the surface to positive increasing the hydrophilicity, while a neutral state is provided at pH 7.4 to form hydrophobicity of aggregation sultone group. The aggregation predominantly decreased the fluorescence of FNP via the aggregation caused quenching (ACQ) phenomenon guiding fluorescent decay via non-radiative pathways to emit light on the condensed phase, reducing the fluorescent properties.[32] Into that hydrophobicity sites, the IR825 were loaded to improve their quenching behaviour via FRET system and simultaneous photo-thermal effect. On the acidic environment, the sultone group in FNP opened which cause the FNP fluorescent restores and release the IR825 far away from FNP surface. Finally, the there are no relationship between IR825 release and switch ON behaviour of FNP. Based on these results, we hypothesized that the FNP-I would show no fluorescence in normal cells, but would show fluorescence when incorporated into acidic cancer cells. Therefore, the designed FNP-I are suitable for use as a biosensor for guided bioimaging tracking through a fluorescent on/off assay.

Figure 3 (a, b) shows the time dependence of the photoluminescent intensity and particle size of FNP-I under different pH treatments. The quenching of fluorescence at pH 7.4 for both sample remained constant, whereas at pH 6 and 6.8, the photoluminescence increased gradually over the first 40 minutes and was fully recovered after 1 hour, when measured at fixed 360 nm excitation and 500 nm emission wavelengths (Figure 3a). The FNP-I cannot recover as a fluorescent intensity of only FNP even the IR825 released because we observed in same solution without removed the IR825 compartment. Therefore, the presence IR825 disturbed the FNP fluorescence profile. The interaction of the ionic complex is easily broken in response to changes in the pH of the solution through deprotonation and protonation processes. These results indicated that our smart nanocarrier would only require 20 min to detect cancer cells. In addition, we also analyse the IR825 emission dependent on time to confirm the release performances. As shown in Figure S6a, at 0 min whole IR825 quantities was trapped inside the FNP under all pH conditions showed low intensity of fluorescence; however after some period time the IR825 emission gradually increases under acid condition but steady under physiological pH. Figure 3b shows that at pH 7.4, the particle size of the FNP-I remained constant, whereas at pH 6 and 6.8, the particle size decreased over time. This confirmed that at neutral pH, IR825 is retained in the core, yet at acidic pH, the FNPs lose their hydrophobicity and release IR825 into solution. In addition, the fluorescence lifetime of FNP-I (Figure 3(c)) was found to be 1.3 ns at pH 7.4, which recovered to 10.0 ns and 10.1 ns at pH 6.0 and 6.8, respectively, implying the fluorescence of the FNP compartment. This means that the FNP-I showed a shorter fluorescence lifetime than FNP because of the quenching effect through FRET.[30] The zwitterionic structure on the FNP core was expected to easily switch between a hydrophilic state and a slightly hydrophobic state in response to pH changes. Therefore, we also analyzed the reversibility behavior through cycles of reversible fluorescence (ON and OFF) of the zwitterionic FNP-I by cycling between pH 6.8 to 7.4 (Figure 3 (d)). They shows reversible hydrophobic of zwitterion by the fluorescence remained stable at pH 7.4 whereas after the first pH decrease to 6.8 the fluorescence switch on occurs, expecting all the IR825 to be released into solution then the reversibility observed is that of the naked FNP and apart from the first cycle, is not affected by IR825.

View Article Online
DOI: 10.1039/C7NR07900A

To combat cancer, the use of PTT agents, as a therapeutic approach using photothermolyis, is a promising method to completely destroy cancer cells and prevent recurrence. It has been reported that when the local hyperthermia of the PTT agent reaches

the 40 ^{o}C or more, it is enough to destroy tumors area within an exact temperature range for a precise period of time by following mechanism.[33] The intrinsic pathway of cell death based PTT activity is mostly activated by cell stress, such as DNA damage and heat shock and mediates cell response to activate the molecules Bak and Bax for mitochondrial outer membrane permeabilization.[34] Finally, some enzyme activities is blocked and ultimately results in the death and apoptosis of the cell. In another mechanism possibility, PTT activity inside cell can produce cellular necrosis to rupture the cell membrane and lead to pro-inflammatory responses that are detrimental to treatment success.[34]

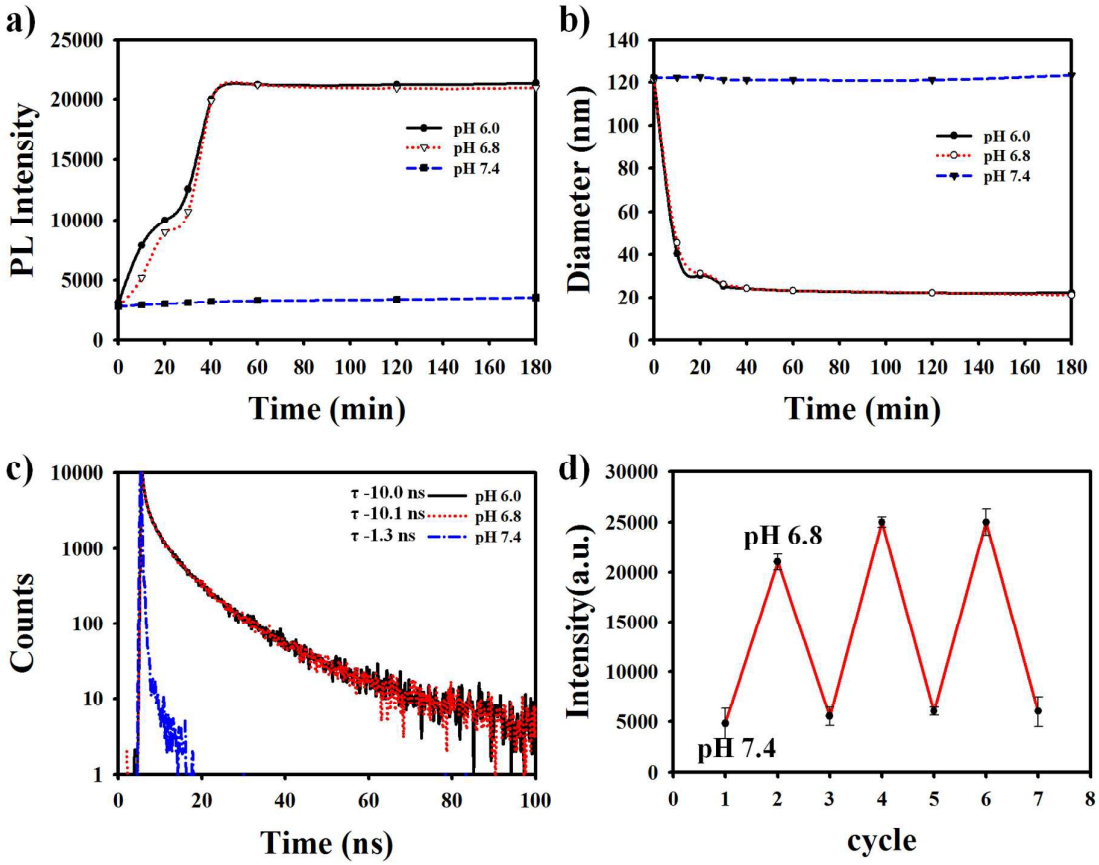

Figure 3. (**a**) Photoluminescence (PL) intensity of FNP and FNP-I at different pH at fixed 360 nm excitation and 500 nm emission wavelengths. (**b**) Dynamic Light Scattering (DLS) measurement of the size of FNP-I in different pH solution. (**c**) Fluorescence decay time curve of FNP-I at an excitation wavelength of 360 nm of wavelength. The τ value indicates respective fluorescence lifetime [FNP concentration 1 mg/mL]. (**d**) Reversible behavior of FNP-I nanoparticles upon cycling the pH between 6.8 and 7.4 at the maximum emission wavelength as a function of the cycle number. FNP, fluorescent nanoparticle; FNP-I, FNP loaded with IR825.

Several studies have shown that functionalized IR825 releases a considerable amount of heat in response to NIR illumination.[35, 36] In this study, the FNP-I also generated sufficient heat (ΔT = ~40 °C) under acidic conditions, which as probably caused by the release of the IR825 into solution, whereas there was little response to NIR light of FNP-I at pH 7.4 (ΔT= ~2 °C), as shown in Figure 4a and Figure S6b. It was clearly showed that under neutral condition the FNP-I showed low photothermal effect because IR825 remained trapped in the FNP core via hydrophobic interaction with ionic complex of sultone and cationic amine. This might be because when the IR825

View Article Online
DOI: 10.1039/C7NR07900A

encapsulated into the FNP core, the IR825 cannot strongly absorb the NIR light, resulting in low response to the electron excitation and the heat conversion. Moreover, we studied possible photothermal effects during NIR light exposure at various concentrations (0.1 to 1 mg/mL) of FNP-I at acidic pH (Figure S7). The NIR-irradiated FNP-I showed increasing of temperature dependent on increasing of concentration. This might be because in the high concentration, the prepared FNP contain also a lot of IR825 amount which will release from FNP surfaces under acidic pH condition to induce the heat conversion by NIR irradiation. Differ from acidic pH, the temperature elevation pattern under basic condition showed no obvious changed for all concentration of FNP-I, indicating IR825 trapping. As comparison, we investigated the thermal release of IR825 alone in ethanol solution on Figure S7a which revealed same temperature elevation profile under all different pH solution. Next, we monitored the release profile of IR825 over time to verify the amount of IR825 released under different pH conditions. Under acidic conditions, almost 100% of IR825 was released in during the first 1 h, whereas at physiological pH, no IR825 was released. These results were consistent with the quenching profiles; the acidic pH makes the zwitterions hydrophilic, causing disaggregation and release of IR825 into the solution, where, in response to NIR light, the thermal energy increases. When FNP-I are injected into the bio-compartment, IR825 will be stable in the core of the FNP; however, when taken up into cancer cells, the intracellular acidic pH would cause release of IR825 to generate fluorescence and the release of thermal energy.

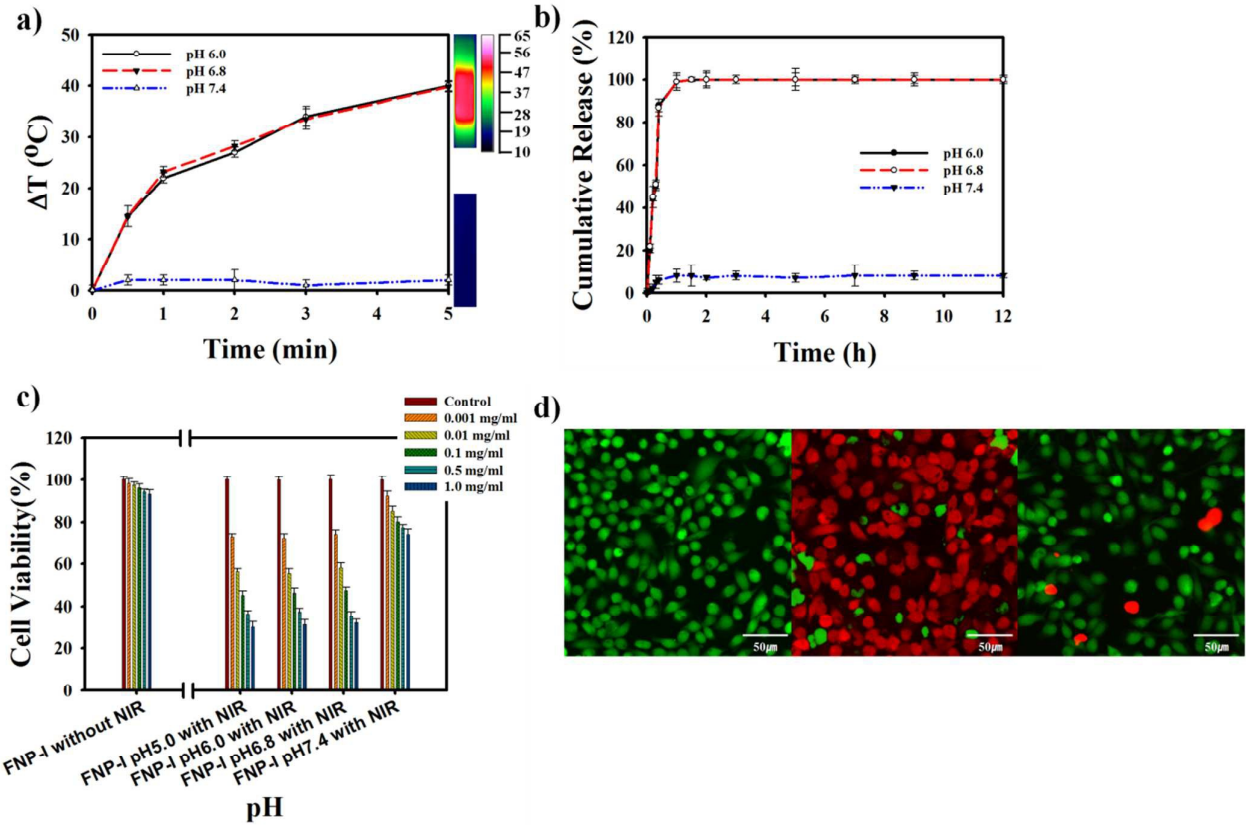

Figure 4. **The temperature elevation curve of an aqueous solution** of (a) FNP-I under NIR irradiation (808 nm laser, 2 W cm-2), at pH values between 6.0 and 7.4. (**b**) *In vitro* release profiles of FNP-I in PBS at pH 7.4, 6.8, and 6.0. (**c**) Cell viability of MDAMB-231 treated with various concentrations (mg/mL) of FNP-I at pH 7.4, 6.8, and 6.0, respectively. (**d**) Live/dead confocal microscopy images using Calcein AM (live, green) and propidium iodide (dead, red) of FNP-I (1 mg/mL) at pH 6.0 (left: only MDAMB-231, middle: with NIR irradiation, right: without NIR irradiation). FNP-I, fluorescent nanoparticle loaded with IR825; PBS, phosphate buffered saline.

View Article Online
DOI: 10.1039/C7NR07900A

For a reliable therapeutic platform, the efficient delivery of the payload and biocompatibility are vital features. To determine *in vitro* biocompatibility and the efficient of NIR irradiated photothermal cancer killing, an MTT assay was performed using MDAMB-231 and MDCK cells. The FNP and FNP-I showed excellent biocompatibility for both normal and cancer cells over a wide concentration range (0.001–1 mg/mL), as shown in Figure S8. The cell viability of MDAMB-231 declined noticeably to 30–45% under mild acidic conditions, while at pH 7.4, nearly 90% of the cells remained alive under NIR irradiation, as shown in Figure 4c. Moreover, the Figure 4 (d) shows the effects of thermal energy inside the cells through fluorescent staining assay. The fluorescence images showed that MDAMB-231 cells treated with FNP-I followed by NIR irradiation selectively increased the number of dead cells (shown in red). Because the IR825 release to the intracellular environment, we further the MTT assay of the treated cell with IR825 dependent on concentration without NIR irradiation shown Figure S9. The IR825 exhibited great biocompatibility and negligible cytotoxicity under dark conditions even at high concentrations up to 1 mg/mL for 24 h of incubation with ~90% MDAMB-231 cancer cells survives, indicating appreciable biocompatibility of IR825 and after release to the cell, IR825 did not give any significant effect to the cell but give hyperthermia effect under NIR exposure. Furthermore, we also analysed the effect of laser irradiance of 2 Wcm^{-2} towards the cell using the same techniques of MTT assay on Figure S10. As a result, cell viability was found to little or no change in response to NIR light, which did not have any adverse effects on MDAMB-231 and MDCK cell.

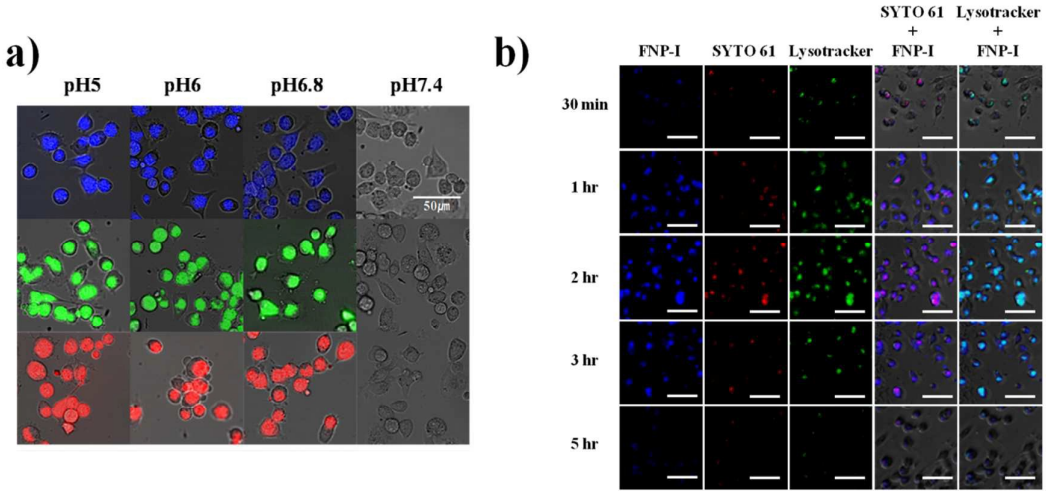

Figure 5. Confocal microscopic fluorescence images of MDAMB-231 cells. (a) Cells treated with FNP-I nanoparticles at different pH values. (b) Cells incubated with FNP-I for 30 min, 1, 2, 4, and 6 h (FNP-I concentration: 1 mg/mL). Blue, FNP-I; Green, LysoTracker; Red, SYTO-61. The scale bars represent a distance of 50 .ac FNP-I, fluorescent nanoparticle loaded with IR825.

The pH responsive characteristic of the FNP-I showed potential for tracking the acidic endosome/lysosome compartments inside cancer cells. In Figure 5, the internalization and confocal imaging of FNP-I in the breast cancer cell line MDA-MB-231 showed strong red, green, and blue fluorescence at the endosomal pH (acidic pH), while fluorescence was not observed at physiological pH (pH 7.4). The results showed that the FNP-I were taken up into the cells and internalized within them. The pH activation could then be used to detect and monitor endosomal escape in living cells. For instance, IR825 released from nanocarriers was observed using LysoTracker (green) and SYTO-61 (red) co-staining methods at different time intervals. The amount of co-localized signal increased incrementally over time, indicating particle accumulation (Figure 5). However, the rate of accumulation slowed down by the 4 h time point. This was due to escape of the FNP nanocarrier from the liposomal vehicle into the cytoplasm, resulting in a minimal fluorescent signal

View Article Online
DOI: 10.1039/C7NR07900A

between 4 and 6 h. In addition to verify the fluorescent "on" performances of FNP-I, we analyzed treated MDAMB-231 cell under pH 6.8 and 7.4 *via* flow cytometry (Figure S11). The FNP-I labeled MDAMB-231 exhibited fluorescence switch off-on under pH 6.8 with fluorescent intensity around 1108 which the initial states under pH 7.4 was found to be low around 476. The result demonstrated the fluorescence peak of the on-state cells was around 2.5 times brighter than that of the off-state in the flow cytometry measurement, indicating excellent pH-responsive fluorescence probes performances to sense intracellular cancer cell. After *in vitro* bioimaging, we verified the *in vivo* delivery of FNP-I in nude Balb/c mice bearing MDAMB-231 cell-derived tumors. FNP-I at 10 mg/kg (body weight) was applied to the tumor through intravenous injection and *in vivo* fluorescent images were capture using an OPTIX MX3. As shown in Figure 6 (a), the brighter fluorescence in the tumor region after 3 h revealed that the fluorescence behavior of FNP-I had been turned on with remarkable cellular uptake, which was indicated by accumulation of FNP-I in the injection area compared with the normal cells. The *in vivo* fluorescence stability was observed at intervals of 0, 1, 2, 3, and 6 h (Figure 6 (b)). At 0 h post injection, we did not observe any fluorescence signal; however, between 1 h and 3 h, the localized FNP-I presented a stable fluorescent signal, indicating that the FNP-I had been internalized via endocytosis into the acid environment of the cells[37], where the quenching effect on IR825 was reversed by their release from the FNP core. Subsequently, because of the inherent photo bleaching and metabolic alteration, the signal decreased at 6 h. Furthermore, the FNP-I accumulated mostly in the tumor, with a slight accumulation in other organs, such as liver, spleen, heart, lung, and kidney.

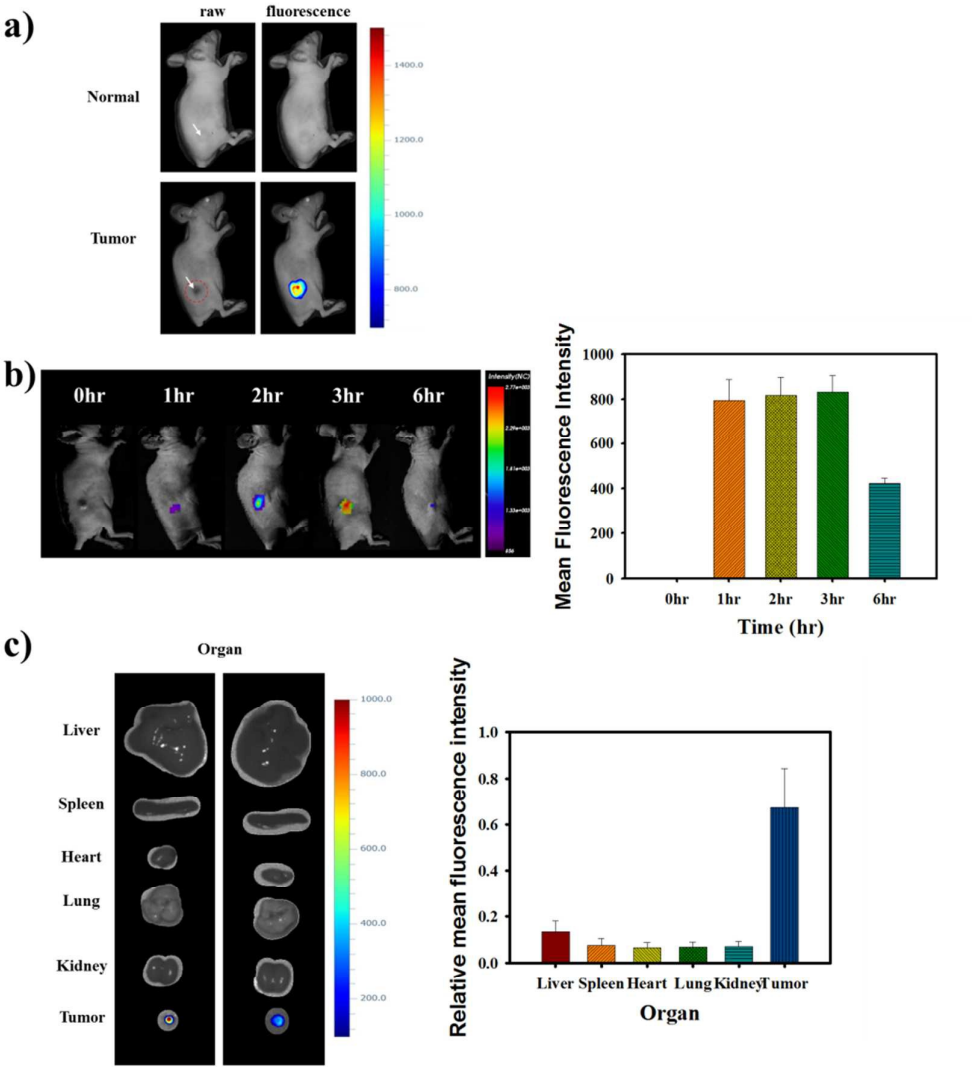

View Article Online
DOI: 10.1039/C7NR07900A

Figure 6. ***In vivo* fluorescence image of FNP-I in Balb/c tumor mice after intravenous injection (10 mg/kg body weight).** (a) Mice after 3 h (b) at intervals of 0, 1, 2, 3, and 6 h after administration. (**c**) Pharmacokinetic profile of FNP-I in MDAMB-231 tumor-bearing mice and *ex vivo* fluorescence image of five major organs and the tumor 3 h post-injection. FNP-I, fluorescent nanoparticle loaded with IR825.

In order to investigate the fact that our prepared FNP system rarely deliver to liver, we further re-analysis the liver organ of treated mice under pH shock (pH 6.4) for 10 min and observed their *ex vivo* fluorescence image in Figure S12. It obvious showed that only slightly FNP nanoparticle goes to liver because after pH shock, we only found weak fluorescence signal recovering. The enhanced tumor localization and intracellular uptake of FNP-I into MDAMB-231 cells could probably be attributed to the EPR[23] and stealth effect[38], thus facilitating the passive accumulation of the nanoparticles in tumor tissue.

The *in vitro* bioimaging results encouraged us to investigate the possibility of treating mice bearing tumors using FNP-I. We intravenously injected an aqueous solution of FNP-I (dose = 10 mg/kg) into balb/c mice bearing MDAMB-231 cell-implanted tumors, and then exposed them to an 808 nm laser at 2 W/ cm2 for 5 min. Measuring the relative tumor volume showed the *in vivo* therapeutic efficacy of FNP-I induced PTT treatment. Figure 7(a) shows that the tumor treated with FNP-I was effectively necrotic after NIR irradiation. In marked contrast, in the control group (mice injected with PBS only), the tumor volume continued to increase. The average size of the tumor in mice in the PBS group was 650 mm^3 after 12 days but was 500 mm^3 on the FNP-I-treated, non-irradiated mice. Interestingly, the tumor was completely suppressed by NIR-irradiated FNP-I nanoparticles after 12 days, to about 100 mm^3, and the tumors were completely ablated at day 12 following the disappearance of tumor in representative images of mice bearing MDAMB-231 tumors. The biocompatibility of FNP-I towards other organs was also evaluated during hyperthermic therapy using hematoxylin/eosin (H & E) staining/histopathological images. As expected, the H&E staining assay showed that FNP-I with NIR irradiation selectively destroyed only the tumor cells without causing noticeable organ damage. No changes in the liver, spleen, heart, lung, and kidney were observed for both the control and FNP-I groups [Figure 7 (b)]. The results suggested that the FNP-I could serve as a pH-responsive, PTT release-based localized cancer therapy under NIR irradiation. In comparison to previous work in the fields of biosensing system which are not so convenient due to the requirement of expensive equipment (chromatography, spectrofluorometric and atomic absorption spectrometry) complicated sample pretreatment and the need of using metal and fluorescent dyes to involve the quenching mechanism,[39, 40] our design demonstrated versatile methods to synthesis the pH-stimuli responsive FNP together with photo-thermal agent IR825 as simultaneous photo-thermal dye and quencher for detection of the cancer cell, controllable selectively delivery and "switch-on/off" visual monitoring therapeutic release of NIR stimuli heat conversion, aiming to outstanding synergetic effect of diagnose and therapy.

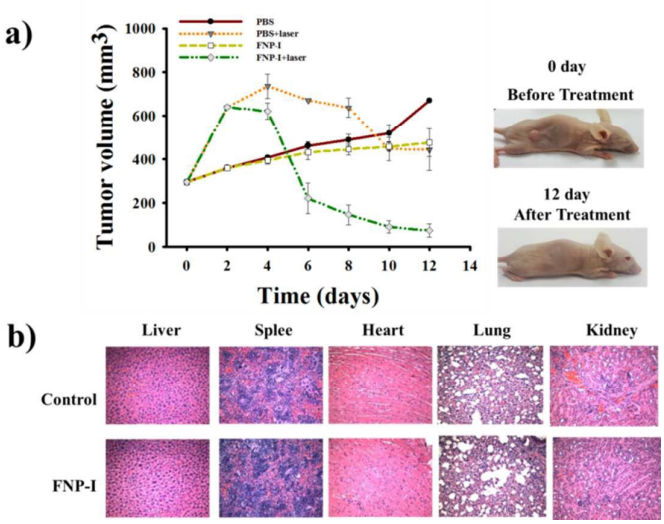

View Article Online
DOI: 10.1039/C7NR07900A

Figure 7. *In vivo* photothermal therapy using FNP-I nanoparticles. (a) Time-dependent tumor growth rate of MDAMB-231 tumor-bearing mice treated with FNP-I and illuminated with laser at a power density of 2 W cm^{-2} with 5 min; digital images of MDAMB-231 tumor-bearing mice at 0 and 12 days. (b) The histology of different organ slices collected from mice after treatment. FNP-I, fluorescent nanoparticle loaded with IR825; PBS, phosphate buffered saline.

Conclusions

In conclusion, a novel pH-sensitive fluorescent probe was successfully developed from IR825-loaded carbonized polymer (FNP-I) for use as a delivery matrix for cancer cell treatment. The fluorescent profile showed strong fluorescence under acidic and basic conditions, but almost no fluorescence at physiological pH because of the zwitterionic behavior of the core of the FNP. By further applying IR825 in the core of the FNP, the FRET effect quenched fluorescence under physiological conditions, which was alleviated in response to acidic cancer cells. It is expected that this feature could be used as "switch-on/off" platform for cancer sensing. In the tumor microenvironment, almost 100% of the IR825 was released from the FNP core to generate high thermal conversion for the complete killing of cancer cells under NIR irradiation. These characteristics resulted in distinct profiles between normal and cancer cells in vitro and were confirmed by confocal imaging. In addition, in vivo fluorescent studies showed that the FNP-I had selective sensitivity and stability inside the cell in response to the tumor environment, indicating good cellular uptake via an enhanced permeability and retention effect. The enhanced photothermal effect caused in vivo tumor growth inhibition, which confirmed the clinical utility of the FNP-I. We concluded that the FNP-I showed selectively drug delivery into the tumor sites through outstanding pH responsivity for the simultaneous diagnosis and treatment of cancer.

Conflicts of interest

The authors state that "There are no conflicts to declare".

Acknowledgements

This research was supported by Grants No. 10062079 and R0005237 from the Ministry of Trade, Industry & Energy (MOTIE) and Korea Institute for Advancement of Technology (KIAT) through the Research and Development for Regional Industry (No R0005303), and the Basic Science Research Program through the National Research Foundation of Korea (NRF) funded by the Ministry of Education (NRF-2017R1A2B2002365).

References

1 Z. Chen, P. Zhao, Z. Luo, M. Zheng, H. Tian, P. Gong, G. Gao, H. Pan, L Liu, A. Ma, H. Cui, Y. Ma, L. Ca, *ACS Nano*, 2016, **10**, 10049.
2 E. J. Moding, M. B. Kastan, D. G.Kirsch, *Nat. Rev. Drug Discov*., 2013, **7**, 526.
3 B. Irène, D. Catherine, C. Patrick, *Adv. Drug Deliv. Rev*., 2012, **64**, 24.
4 S. Jain, D. G. Hirst, J. M. O'Sullivan, *Br. J. Radiol*., 2012, **85**, 101.
5 Z. Lili, W. Hong, H. Bin, Z. Lijuan, T. Tao, C. Haiqiang, H. Xinyu, Z. Zhiwen, G. Shengrong, L. Yaping, *Theranostics*, 2016, **6**, 762.
6 H. Xiaohua, H. E. Ivan, Q. Wei, A. E. Mostafa, *J. Am. Chem. Soc*., 2006, **128**, 2115.
7 H. Jing, L. Jinru, J. Wenfeng, Y. Liangming, L. Xiaoqin, J. Long, T. Yong, *Int. J. Nanomedicine*, 2014, **9**, 517.
8 L. Dong, Y. Fang, G. Ning, *Theranostics*, 2016, **9**, 1306.
9 S. Yigang, Y. Yingwen, D. Yongzhong, H. Xuan, H. Jiabei, Y. Jian, Y. Hong, H. Fuqiang, *Mol. Pharmaceutics*, 2015, **12**, 1193.
10 K. Yasumasa, O. Shigeyuki, M. Chihiro, M. Yojiro, S. Atsuko, M. Toyonobu, B. Yuh, *Cancer Cell Int*., 2013, **13**, 89.
11 Khoerunnisa, E. B. Kang. Z. A. I. Mazrad, G. Lee, I, In. S. Y. Park, *Mater. Sci. Eng. C*, 2017, **7**, 1064.
12 T. Mosaiab, C. Shin, P. H. Choi, G. Shin, S. Lee, K. H
. Choi, E. S. Yoo, J. Lee, I. In, S. Y. Park, *New J. Chem*., 2013, **37**, 3845.
13 J. Lai, B. P. Shah, E. Garfunkel, K. B. Lee, *ACS Nano*, 2013, **7**, 2741.
14 L. Feng, C. Tong, Y. He, B. Liu, C. Wang, J. Sha, C. Lü, *Journal of Luminescence*, 2014, **146**, 502.
15 S. M. Sharker, S. M. Kim, J. E. Lee, J. H. Jeong, I. In, K. D. Lee, H. Lee, S. Y. Park, *Nanoscale*, 2015, **7**, 5468.
16 Z. A. I. Mazrad, E. B. Kang, I. In, S. Y. Park, *Luminescence*, 2017, 1.
17 Y. Chen, P. Xu, M. Wu, Q. Meng, H. Chen, Z. Shu, J. Wang, L. Zhang, Y. Li, J. Shi. *Adv. Mater.,* 2014, **26**, 4294.
18 X. Liu, G. Yang, L. Zhang, Z. Liu, Z. Cheng, X. Zhu, *Nanoscale*, 2016, **8**, 15323.
19 Y. Zhang, C. Y. Ang, Y. Zhao. *Polym. J,* 2016, 48, 589.
20 K. Wang, Y. Zhang, J. Wang, A. Yuan, M. Sun, J. Wu, Y. Hu, *Sci. Rep.,* 2016, **6**, 27421.
21 D. Hu, C. Liu, L. Song, H. Cui, G. Gao, P. Liu, Z. Sheng, L. Cai, *Nanoscale*, 2016, **8**, 17150.

View Article Online
DOI: 10.1039/C7NR07900A

22 B. Pravin, D. Zhifei, *Adv. Healthcare Mater*., 2017, 1-23.
23 K. Greish, *Methods Mol. Biol.,* 2010, **624**, 25.
24 L. Cheng, W. He, H. Gong, C. Wang, Q. Chen, Z. Cheng, Z. Li, *Adv. Funct. Mater.,* 2013, **23**, 5893.
25 J. A. Nam, A. A. Nahain, S. M. Kim, I. In, S. Y. Park, Acta Biomaterialia, 2013, **9**, 7996.
26 Z. A. I. Mazrad, I. In, K. D. Lee, S. Y. Park, *Biosens. Bioelectron*., 2017, **89**, 1026.
27 Z. A. I. Mazrad, C. A. Choi, Y. M. Kwon, I. In, K. D. Lee, S.Y. Park, *ACS Appl. Mater. Interfaces*, 2017, DOI: 10.1021/acsami.7b10688.
28 Khoerunnisa, Z. A. I. Mazrad, I. In, S.Y. Park, *Biosens. Bioelectron.,* 2017, **90**, 394.
29. S. Bhattacharyya, B. Konkena, K. Jayaramulu, W. Schuhmann, T. K. Maji, *J. Mater. Chem. A*, 2017, **5**, 13573.
30 J. W. Arbogast, C. S. Foote, M. Kao, *J. Am. Chem. Soc*., 1992, **6**, 2277.
31 X. Wang, L. Cao, F. Lu, M. J. Meziani, H. Li, G. Qi, B. Zhou, B. A. Harruff, F. Kermarrec, Y. P. Sun, *Chem. Commun*., 2009, **0**, 3774.
32 C. T. Chien, S. S. Li, W. J. Lai, Y. C. Yeh, H. A., Chen, I. S. Chen, L. Chen, K. H. Chen, T. Nemoto, S. Isoda, M. Chen, T. Fujita, G. Eda, H, Yamaguchi, M. Chhowalla, C. W. Chen, *Angew. Chem. Int. Ed.*, 2012, **51**, 6662.
33. Z. Behrouzkia, Z. Joveini, B. Keshavarzi, N. Eyvazzadeh, R. Z. Aghdam, *Oman Med J.,* 2016, **31**, 89.
34. J. R. Melamed, R. S. Edelstein, E. S. Day, *ACS Nano*, 2015, **9** , 6.
35 Y. Zhang, C. Teh, M. Li, C. Y. Ang, S. Y. Tan, Q. Qu, V. Korzh, Y. Zhao, *Chem. Mater.* 2016, **28**, 7039.
36 E. B. Kang, J. E. Lee, J. H. Jeong, G. Lee, I. In, S. Y. Park, *J. Ind. Eng. Chem.,* 2016, **33**, 336.
37 A. K. Varkouhi, M. Scholte, G. Storm, H. J. Haisma*, J. Control Release*, 2011, **151**, 220.
38 N. J. Butcher, G. M. Mortimer, R. F. Minchin, Nat. Nanotech., 2016, **11**, 310.
39. W. Lu, X. Qin, S. Liu, G. Chang, Y. Zhang, Y. Luo, A. M. Asiri, A. O. Al-Youbi, X, Sun. *Anal. Chem.,* 2012, **84**, 5351–5357.
40. M. Tuerhong, Y. Xu, X. B. Yin, *Chinese J. Anal. Chem.,* 2017, **45**, 139.